Crystal Structures of Deoxy and CO-Bound *bj*FixLH Reveal Details of Ligand Recognition and Signaling‡

Jason Key§ and Keith Moffat*,§,||

Department of Biochemistry and Molecular Biology, Consortium for Advanced Radiation Sources, and Institute for Biophysical Dynamics, University of Chicago, Chicago, Illinois 60637

Received September 22, 2004; Revised Manuscript Received November 23, 2004

ABSTRACT: Rhizobia directly regulate the expression of genes required for symbiotic nitrogen fixation in response to oxygen concentration via the sensor protein FixL. The N-terminal PAS domain of FixL contains a histidine-coordinated heme and regulates the activity of its effector domain, a C-terminal histidine kinase, in response to binding of oxygen and other ligands at the heme. To further investigate ligand-induced inhibition of FixL, we have determined the crystal structures of the heme domain in both the deoxy state and bound to carbon monoxide, a weak inhibitor of FixL kinase activity. Structures collected at room temperature are presented in each state from two crystallographic space groups at 1.8 and 2 Å resolution. These structures reveal displacement of the residues of the H_β and I_β strands by Leu236 upon CO binding, and this structural change propagates more than 15 Å to a region of the structure implicated in signal transduction in PAS proteins. Displacement of residues Ile215, Ile216, and Gly217 in the FG loop is also evident, accompanied by the movement of heme propionate 6 upon change in iron ligation. CO binding increases the temperature factors in the FG loop of the protein and disorders the side chain of Arg206, a conserved residue involved in the FG loop switch mechanism. We relate these results to structural changes in other PAS sensor domains and their involvement in catalytic control.

Nitrogen fixation is an inherently anaerobic process. As a consequence, nitrogen-fixing Rhizobia have evolved complex regulatory control systems for dealing with a gradient of decreasing oxygen concentration during root nodule development (*1*). These bacteria regulate expression of the genes responsible for nitrogen fixation and microaerobic/anaerobic respiration in response to molecular oxygen. The protein FixL, a dimeric, heme-based oxygen sensor, is directly responsible for this oxygen-dependent regulation. FixL belongs to the large family of bacterial two-component sensors (*2*), modular proteins typically composed of a sensory domain and an enzymatic signaling or effector domain. FixL is comprised of a C-terminal histidine kinase domain and an N-terminal sensory domain that contains covalently bound heme (*3*). This N-terminal domain belongs to the PAS[1] domain structural superfamily, a ubiquitous protein sensory module found in all kingdoms of life (*4*−*6*). PAS domains are characterized by a conserved α/β fold and are responsible for protein dimerization (*7*) and recognition of various stimuli via a chemically diverse array of prosthetic groups (*8*−*10*). Heme-based PAS sensor proteins have recently emerged as a distinct subclass of signaling modules that are able to detect oxygen, carbon monoxide, and possibly cellular redox state (*9*, *11*−*13*).

In FixL, the N-terminal PAS domain controls the activity of the C-terminal histidine kinase. When the heme of the PAS domain is unliganded, the kinase is active and phosphorylates the two-component system partner of FixL, the DNA-binding response regulator FixJ, thus stimulating transcription of the *fixK* operon (*14*). When oxygen is bound to the heme of the FixL sensory domain, kinase activity is suppressed. This results in downregulation of the expression of nitrogen fixation genes to prevent the sacrifice of oxygen-sensitive nitrogenase. Gilles-Gonzalez and colleagues (*15*) originally proposed a spin-state mechanism for regulation of FixL in which activity of the kinase domain is regulated by the spin state of the heme iron. Recently, they have shown that ligand-induced regulation of the kinase by the heme−PAS domain is more complex (*16*, *17*). Diatomic ligands can be divided into strong and weak inhibitors; O_2 and CN act as strong inhibitors of FixL kinase activity and CO and NO as weak inhibitors.

Crystallographic studies of the isolated heme−PAS domains of FixL from *Bradyrhizobium japonicum* (*bj*FixLH) and *Sinorhizobium meliloti* (*sm*FixLH) (*17*−*21*) have explored the mechanism of signal recognition. Crystal structures of *bj*FixLH bound to the low-spin ligands CN and O_2, strong inhibitors of FixL phosphorylation, show that ligand binding is accompanied by a structural change in the FG loop of the

‡ Protein structure coordinates have been deposited in the Protein Data Bank as entries 1XJ2, 1XJ3, 1XJ4, and 1XJ6.

* To whom correspondence should be addressed: Department of Biochemistry and Molecular Biology, University of Chicago, Chicago, IL 60637. Phone: (773) 702-2116. Fax: (773) 702-0439. E-mail: moffat@cars.uchicago.edu.

§ Department of Biochemistry and Molecular Biology.

|| Consortium for Advanced Radiation Sources and Institute for Biophysical Dynamics.

[1] Abbreviations: PAS, acronym formed from the names of the eukaryotic proteins period (PER), aryl hydrocarbon receptor nuclear translocator (ARNT), and simple-minded (SIM); *bj*FixLH, heme−PAS domain of the FixL protein from *B. japonicum*; *sm*FixLH, heme−PAS domain of the FixL protein from *S. meliloti*; *ec*DOSH, heme−PAS *E. coli* protein DOS.

10.1021/bi047942r CCC: $30.25
Published on Web 03/05/2005

protein, termed "the FG loop switch" (*18*−*20*). This change is caused by the reorientation of the side chain of Arg220 in the heme pocket, in formation of a hydrogen bond with the bound ligand. Smaller structural changes in the FG loop were reported upon binding of NO (*19*). Curiously, the low-spin CO-bound structure was reported to be nearly identical to the structures of met-*bj*FixLH (high-spin ferric heme iron) and deoxy-*bj*FixLH (high-spin ferrous heme iron) (*19*, *20*). These findings led Gong and colleagues (*20*) to propose a mechanism for regulation based on the structural change in the FG loop of the protein. Conversion of the domed, high-spin heme in the deoxy state to a planar low-spin hexacoordinate state upon ligand binding changes the heme stereochemistry and displaces the heme propionate side chains. Displacement of the carboxylate of heme propionate 7 weakens its salt bridge to the side chain of Arg220, prompting replacement of this group at the propionate with the side chain of Arg206. Arg220 then moves into the binding pocket where it forms a hydrogen bond with the bound ligand, creating a steric clash with Ile215 and producing a 2 Å shift in the FG loop. This structural change presumably results in kinase inhibition through a mechanism that is not understood.

An alternative mechanism has been proposed whereby conformational change is driven by the steric interaction between the bound ligand and the distal hydrophobic residues (*21*, *22*). The ligand binding pocket of FixL contains three conserved hydrophobic side chains, termed the hydrophobic triad. Each of these side chains must be displaced to bind ligand, and this displacement gives rise to signal in the form of structural change within the protein. This model is supported by mutational analysis of FixL by Mukai and colleagues (*23*) which reveals that *sm*FixLH Ile209 and Ile210 mutants (corresponding to Ile215 and Ile216, respectively, in *bj*FixLH) are deficient in ligand recognition and signaling.

Dunham and co-workers (*17*) showed that the R220A mutant of FixL has a dramatically lowered affinity for O_2. CO binding was unchanged in this mutant, however, and curiously, CN-bound R220A mutants retain some ability to weakly inhibit FixL in the absence of the FG loop switch. This finding suggests that the FG loop switch cannot be the sole factor in kinase regulation (*17*). Thus, the mechanism of the conformational change in the FG loop and the process of ligand-induced regulation of kinase activity are complex, and remain the subject of debate.

To investigate the structural events associated with ligand recognition and signaling in *bj*FixLH, we determined crystal structures in the deoxy form and in complex with carbon monoxide at a higher resolution (1.8−2.0 Å) than in previous structures (2.4 Å) (*20*). The CO complex is of considerable interest because prior work has shown that CO binding does not evoke the substantial FG loop conformational change observed for the oxygen-bound species (*20*) and, in fact, shows the least degree of conformational change of all ligand-bound structures of *bj*FixLH, yet CO binding results in appreciable inhibition of FixL activity (*16*). We examine CO-bound structures to detect conformational changes responsible for the weaker levels of inhibition in intact *bj*FixLH by CO. Changes that are important for signal recognition are likely to be found outside the FG loop region. We crystallized *bj*FixLH in two crystal forms: rhombohedral crystals similar to those described previously (*19*) and a novel monoclinic form. The two crystal forms provide an opportunity to assess the effects of crystal solvent content and lattice packing on the structure and ligand binding. Because the structural changes associated with CO binding are expected to be quite small, high-resolution structures are necessary; all structures in this study were determined to <2 Å resolution, in contrast to earlier ligand-bound structures determined at 2.4 Å resolution (*18*). Data were collected at room temperature to best approximate physiological conditions and to provide a basis for subsequent time-resolved studies of CO photolysis and rebinding (manuscript in preparation).

MATERIALS AND METHODS

Expression, Crystallization, and Microspectrophotometry. The *bj*FixLH protein was expressed and purified as described previously (*24*). This expression construct encodes residues 140−280 of *bj*FixL. Additional purification by ion exchange chromatography on high-performance Q-Sepharose anion exchange resin (Pharmacia) was performed prior to crystallization. Rhombohedral crystals of *bj*FixLH were grown by hanging drop vapor diffusion against a 1 mL reservoir containing 3.9 M NaCl, 1% PEI, and 50 mM CAPSO (pH 9.0). The hanging drop contained 5 μL of purified *bj*FixLH at a concentration of 55 mg/mL mixed 1:1 with mother liquor. Monoclinic crystals were grown in the same fashion using a mother liquor containing 3.9 M NaCl, 3% ethylene glycol, and 50 mM Tris (pH 8.5). All crystals were grown in the oxidized met form. CO−*bj*FixLH crystals of the monoclinic form were prepared by first reducing the met crystals with 200 mM ascorbate in CO-saturated mother liquor for at least 4 h. Reduced crystals were mounted in glass capillaries containing CO-saturated mother liquor to which a few crystals of sodium dithionite had been added. The capillaries were thoroughly flushed with CO and quickly sealed with epoxy. CO−*bj*FixLH crystals of the rhombohedral crystal form were prepared in the same way except that sodium dithionite was used in place of ascorbate. To prepare deoxy crystals, capillaries were flushed with nitrogen gas in place of carbon monoxide. Microspectroscopy on crystals was performed using a single-crystal microspectrophotometer constructed in our laboratory (*25*). No oxidation or loss of CO was observed over several weeks from crystals mounted in this manner. All crystals were mounted a few days prior to data collection.

Data Collection and Reduction. Monochromatic oscillation X-ray data were collected at the BioCARS 14 BM-C beamline at the Advanced Photon Source (Argonne National Laboratory, Argonne, IL) on an ADSC Quantum4 CCD detector at 14 °C and processed using DENZO/SCALEPACK (*26*). Molecular replacement was conducted using EPMR (*27*) with the previously determined met-*bj*FixLH [Protein Data Bank (PDB) entry 1DRM] structure as a search model (*18*). Rigid body refinement, simulated annealing refinement, individual isotropic *B*-factor refinement, and conjugate-gradient minimization were performed using CNS (*28*). To minimize model bias, the positions of FG loop residues 209−220 were refined manually using $2F_o - F_c$ and $F_o - F_c$ simulated annealing composite omit maps and $2F_o - F_c$ and $F_o - F_c$ simulated annealing omit maps in the two CO-bound structures. Model building was carried out using O and

Table 1: Data Processing and Refinement Statistics

	CO	deoxy	CO	deoxy
space group	*C*2	*C*2	*R*32	*R*32
unit cell parameters				
a (Å)	81.13	81.10	128.34	128.69
b (Å)	59.64	59.92	128.34	128.69
c (Å)	59.46	59.57	58.52	58.75
β (deg)	111.75	111.51	111.51	111.51
no. of molecules per asymmetric unit	2	2	1	1
solvent content (%)	43.4	43.4	59.3	59.3
resolution range (Å)	40−1.8	40−1.9	40−2.0	40−1.9
no. of crystals	4	3	2	2
no. of observed reflections	142295	101482	172175	221546
no. of unique reflections	23041	19749	11779	13604
overall redundancy	6.18	5.14	14.61	16.29
$I/\sigma I$ (highest-resolution shell)	25.6 (1.94)	17.7 (2.1)	22.1 (2.14)	17.9 (2.3)
R_{merge}[a] (%) (highest-resolution shell)	7.7 (46.5)	5.9 (44.7)	3.1 (48.8)	3.1 (43.1)
completeness (%) (highest-resolution shell)	94.0 (69.0)	93.7 (60.2)	93.4 (73.4)	92.1 (65.1)
R_{cryst}[b] (%)	21.7	20.7	21.2	20.4
R_{free}[c] (%)	24.7	24.1	25.6	24.4
rmsd for bond distances (Å)	0.0081	0.0078	0.0092	0.0081
rmsd for bond angles (deg)	1.39	1.68	1.88	1.63

[a] $R_{merge}(I) = \sum_h\sum_i|I_i - I|/\sum_h\sum_i I$, where I is the mean intensity of the i observations of reflection h. [b] $R_{cryst} = \sum|F_{obs} - F_{calc}|/\sum|F_{obs}|$, where F_{obs} and F_{calc} are the observed and calculated structure factors, respectively. [c] R_{free} is the same as R_{cryst}, calculated from a randomly selected subset of the data excluded from refinement. R_{free} was calculated using 6.5% of the reflections for the *C*2 structures and 9% for the *R*32 structures.

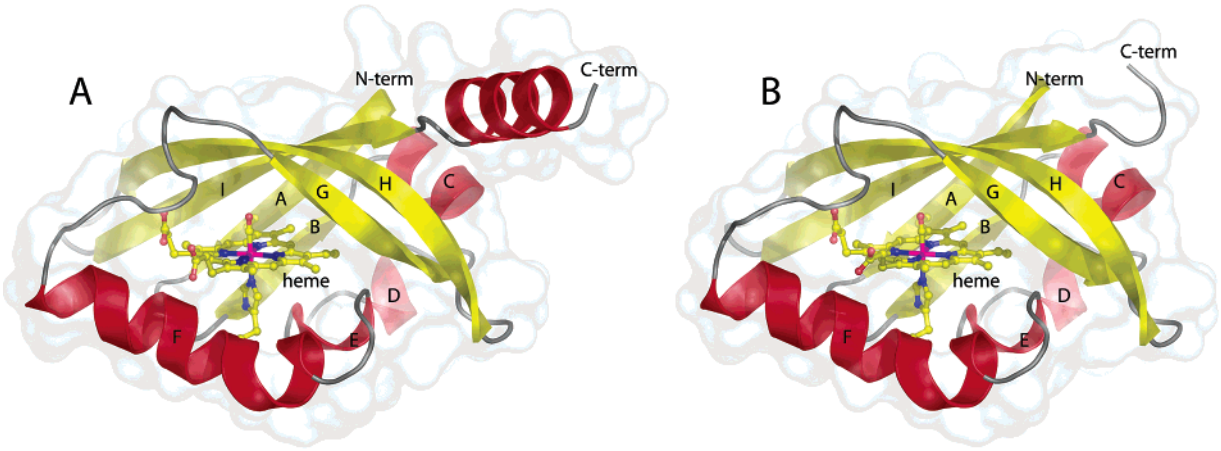

FIGURE 1: Ribbon diagrams of the CO complex of *bj*FixLH from the *R*32 (A) and the *C*2 (B) crystal forms.

XtalView (*29*, *30*). Structure alignments were made with CCP4 (*31*), and figures were prepared using Ribbons (*32*), Xtalview, and Pymol (*33*).

RESULTS

Protein Structure. Six independent structures of *bj*FixLH, three each in the CO and deoxy states at 1.8, 1.9, and 2.0 Å resolution, were refined to crystallographic *R*-factors between 20.7 and 21.7% (Table 1). The *R*32 crystal form contains one molecule per asymmetric unit consisting of residues 154−269 and is similar to the *bj*FixLH structures determined previously (Figure 1A) (*19*). The *C*2 crystal form contains two monomers, *C*2A and *C*2B, in the asymmetric unit. The *C*2A model consists of residues 154−255, while the *C*2B model has density for residues 152−255. Both monomers in the *C*2 form lack density for the extended C-terminal helix found in the *R*32 model (residues 258−269), which creates a 3-fold symmetrical crystal contact (Figure 1B). With the exception of the absence of this C-terminal helix, the structures are very similar, as expected. Least-squares alignment of all atoms among the six models confirms that the structures are in close agreement with an all atom rmsd of ~0.7 Å between each model and each of the other five models (two each in the *C*2 form for CO and deoxy and the CO and deoxy *R*32 models). Two regions of the protein structure differ among the three models, the flexible FG loop and the HI turn between the H_β and I_β strands. These differences are imposed by the crystal lattice and are independent of the protein ligation state. They are located at the C-terminal end of the FG loop at residues Gly217 and Ile218, and at the beginning of the FG loop at residues Thr210 and Ser211. The HI turn, a tight turn between the H_β and I_β strands which contains two neighboring glycine residues, differs in the *C*2 and *R*32 models but is identical in the *C*2A and *C*2B structures. The structural difference is greatest at residues Ile238−Glu246, which are displaced by 0.7 Å between the *R*32 and *C*2 forms which appears to be caused by the intermolecular interaction between the two monomers in the *C*2 asymmetric unit. These differences in the FG loop and HI turn suggest that the conformation of these regions is readily variable and subject to the influence of crystal lattice contacts. In the *bj*FixLH structures, most residues of the protein are ordered with the exceptions of the side chains of Arg254 and Gln261 in the *R*32 CO

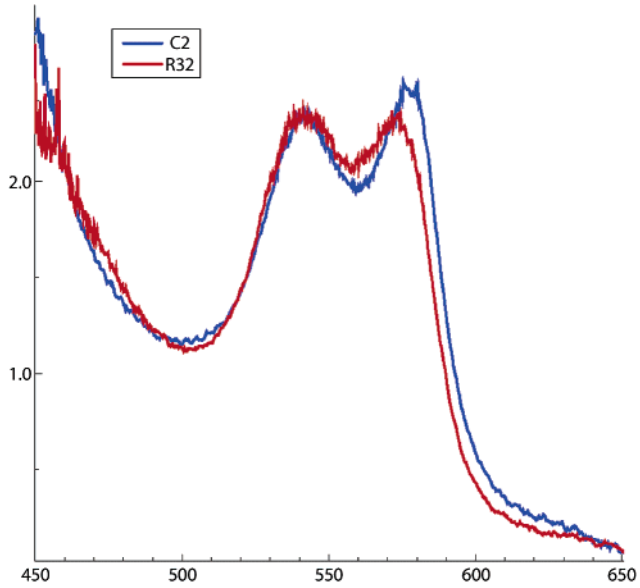

FIGURE 2: Absorbance spectra of capillary-mounted *bj*FixLH crystals in the *C*2 (blue) and *R*32 (red) forms after reduction and addition of CO. The differences in peak height between the two forms arise from polarization of the xenon lamp beam.

structure, Arg206 in both the *R*32 CO and *C*2B CO structures, and Arg174 in the *C*2A deoxy structure.

CO Binding in bjFixLH. Previous studies (*18*) required high-pressure methods for preparation of CO−*bj*FixLH crystals, but we did not find these to be necessary; simple reduction of met-*bj*FixLH crystals followed by transfer to a CO-saturated solution was sufficient. To confirm the presence of bound CO in our *bj*FixLH crystals prior to X-ray data collection, absorbance spectra were collected from both *R*32 and *C*2 crystals after reduction and exposure to CO. These spectra reveal the characteristic spectral features of CO-bound FixLH and confirm the presence of a saturating level of CO and the absence of significant met species in both crystal forms (Figure 2). The $2F_o - F_c$ electron density maps of the heme pocket clearly show bound CO in both the *R*32 and *C*2 forms (Figure 3A,B), and an unliganded, pentacoordinate, domed heme in the deoxy states (Figure 3C,D). Our $2F_o - F_c$, $F_o - F_c$, and F_o(deoxy) − F_o(CO) electron density maps are consistent with a bound CO molecule that is very nearly linear, as has been suggested for CO in heme model compounds (*34*, *35*), inferred from spectroscopic measurements (*36*), and observed in high-resolution crystallographic studies on myoglobin (*37*, *38*). The refined Fe−C−O bond angle is 170.1°, 171.2°, and 169.7° in the *R*32, *C*2A, and *C*2B models, respectively, and the CO is nearly perpendicular to the plane of the porphyrin. Previous crystallographic and EXAFS studies reported significantly lower values of 157° and 156.4° for this angle (*20*, *39*); thus, our CO stereochemistry differs from that reported previously. The largely hydrophobic nature of the *bj*FixLH binding pocket supports a CO geometry similar to that of model compounds; there are no polar distal side chains interacting with CO in *bj*FixLH.

Structural Differences between the CO and Deoxy States and the Effects of Crystal Lattice Contacts. On the basis of the previous study of the CO−*bj*FixLH species (*20*), we expected the structural differences between the CO and deoxy states to be small. We therefore examined F_o(deoxy) − F_o(CO) difference electron density maps which are very sensitive to small changes in structure (*40*). Difference Fourier maps were calculated between the CO and deoxy forms in both space groups using phases calculated from the CO-bound model (Figure 4). Because the structural differences are small, phases from the deoxy model or from true difference phases calculated from the refined CO and deoxy models produce maps that are virtually indistinguishable (data not shown). This approach, when coupled with the examination of the differences in the refined coordinates of the models (Figure 5), allows the subtle effects of CO binding to be readily detected.

Significant conformational differences between the CO and deoxy states are evident in two areas of the protein: the H_β and I_β strands distal to the heme binding pocket and the FG loop (Figure 4). These differences are common to all three molecules except for the FG loop of the *C*2A molecule (discussed below). The most prominent structural differences center on the side chain of residue Leu236 in the H_β strand. In the deoxy state, Leu236 occupies the region directly over the heme iron. This side chain must vacate the ligand binding pocket to accommodate the bound CO, and in so doing, the main chain atoms of Leu236 shift away from the CO along the H_β strand toward its C-terminus. The average rms displacement of the main chain atoms of Leu236 is 0.25 Å in the *C*2A chain, 0.26 Å in the *C*2B chain, and 0.22 Å in the *R*32 structure. This shift displaces the backbone atoms of residues Phe252 and Val253 in the I_β strand with which Leu236 makes hydrogen bonds. A structural domino effect is evident in prominent difference electron density (at $\pm 4\sigma$) that extends from the CO, along the side chain of Leu236, and to the backbone atoms of residues Val253, Arg254, and Asp255 in the I_β strand, more than 15.0 Å from the site of CO binding at the heme iron (Figure 6A).

Difference features indicating structural differences in the FG loop center on residue Ile216 and extend along the backbone of the FG loop to adjacent residues Ile215 and Gly217 (Figure 6B). The main chain rms deviation of Ile215 is 0.3 Å in the *C*2B structure and 0.33 Å in the *R*32 form. The *C*2A monomer does not show significant displacement in the FG loop (discussed below). A prominent difference electron density peak ($+4\sigma$) is visible on the heme propionate 6 side chain which is hydrogen bonded to the backbone amide of residue Ile216. Curiously, propionate 7, which is involved in a salt bridge to the distal residue Arg220 in the oxy structure (*18*), does not exhibit any difference features. Likewise, none are seen on the Arg220 side chain; therefore, the salt bridge to propionate 7 remains intact. The side chain of Arg206 [a conserved residue implicated in neutralizing the charge of the heme propionate group and destabilizing Arg220 (*18*−*20*)] is bound to the main chain carbonyl oxygen of Asp212 in each of the deoxy structures. The temperature factors of Asp212 and the side chain of Arg206 are the highest in the *R*32 and *C*2B models, suggesting that this region of the protein is flexible. The side chain of Arg206 becomes disordered upon binding of CO at room temperature in the *C*2B and *R*32 structures, but remains ordered in the *C*2A monomer. In addition, an ~20% increase in the average main chain temperature factor of the residues of the FG loop is evident in the CO structures of the *C*2B and *R*32 forms compared with the deoxy form. This increase is most pronounced in the last turn of the F helix in residue Asp206,

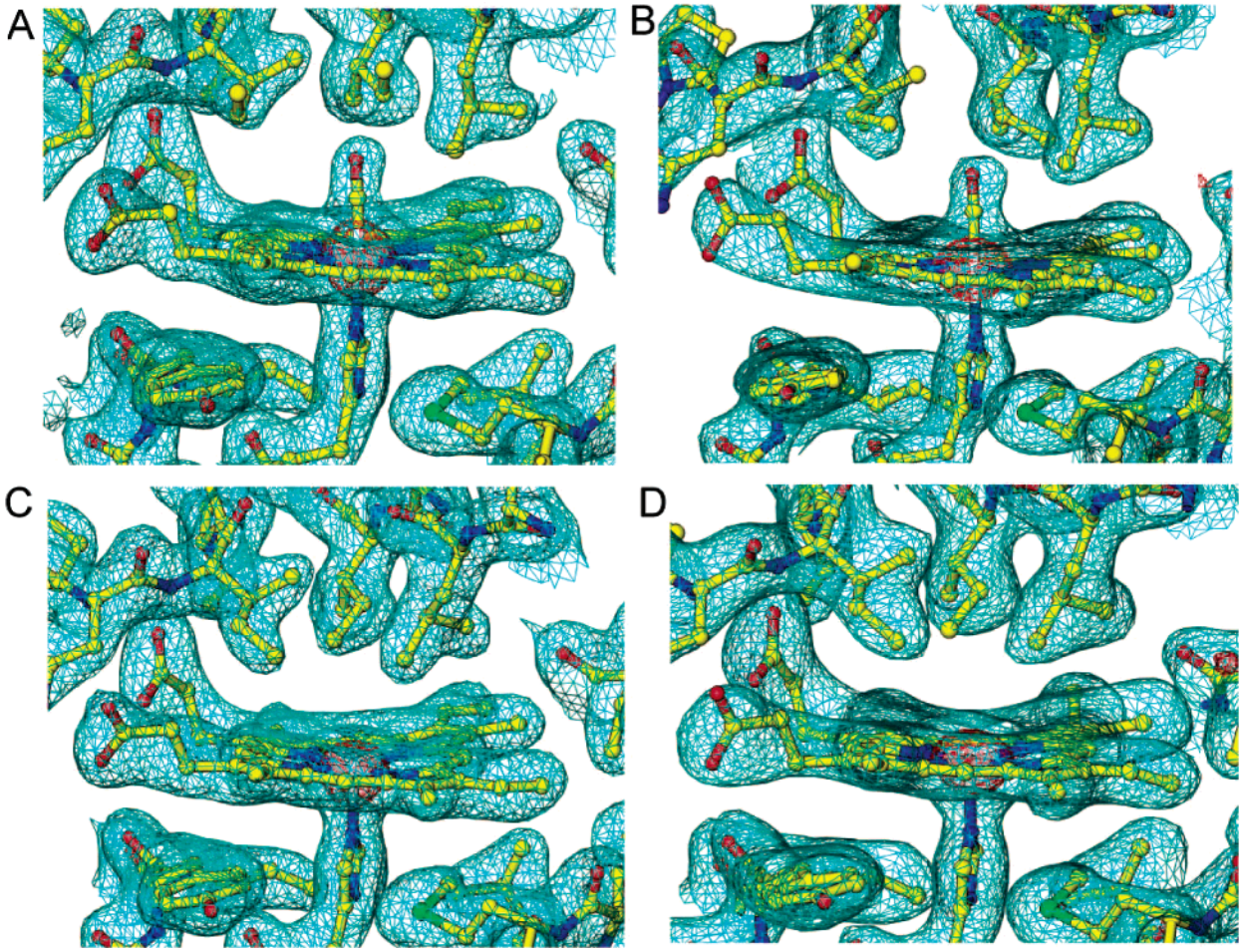

FIGURE 3: $2F_o - F_c$ maps of the heme-binding pocket of *bj*FixLH. (A) *C*2 crystal form with CO bound at 1.8 Å resolution. (B) *R*32 form with CO bound at 2.0 Å resolution. (C and D) Deoxy species from the *C*2 and *R*32 crystal forms at 1.9 Å resolution, respectively. Contours are 1σ (cyan) and 5σ (red).

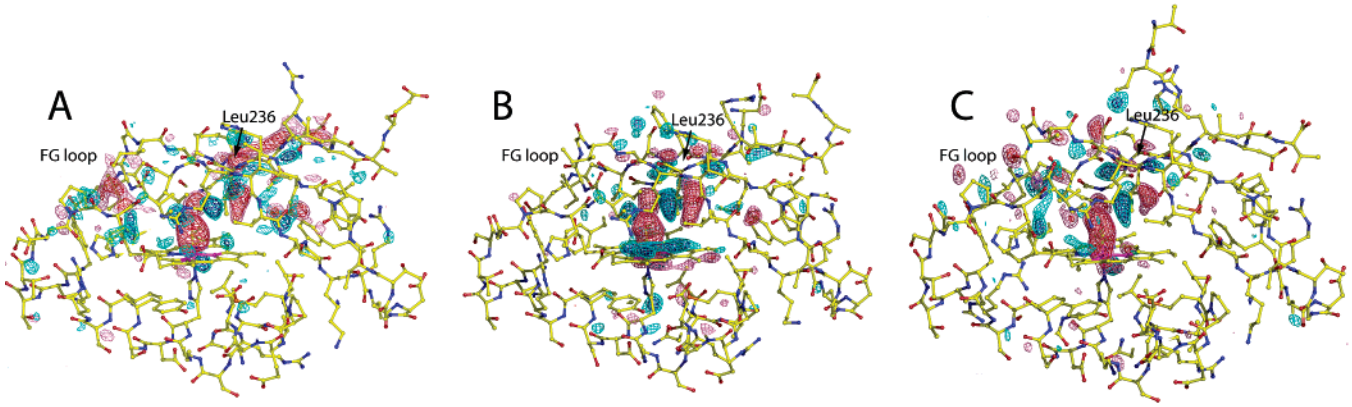

FIGURE 4: F_o(deoxy) − F_o(CO) difference Fourier maps superimposed on the *bj*FixLH model from the *R*32 crystal form (A), the *C*2A monomer (B), and the *C*2B monomer (C) from the *C*2 crystal form. These are contoured at ±3.5σ and ±4.5σ, where σ is the rms value of $\Delta\rho$ across the asymmetric unit. Negative difference density is red, and positive difference density is blue. Differences in electron density are common to the Hβ and Iβ strands of the protein, and to the FG loop of the *R*32 crystal and the *C*2B monomer.

in the FG loop at Asp212, and near the end of the FG loop at residues Gly217 and Ile218.

Different crystal lattice packing in the *R*32 and *C*2 crystal forms gives rise to differences in the CO-induced structural changes. Both monomers in the *C*2 crystal form are more restricted by crystal packing than the monomer in the *R*32 form, and this is evident in two ways. The most prominent lattice-related difference is in the FG loop of the *C*2A monomer, in which a sodium ion is coordinated at the backbone carbonyls of residues Gly217 and Ile218. This contact effectively locks the conformation of the FG loop upon CO binding with interesting consequences. The FG loop and propionate 6 show no difference in position between the CO and deoxy states in the *C*2A model, although heme doming is evident in the refined positions of the heme atoms and in F_o(CO) − F_o(deoxy) difference maps. The side chain of Arg206 remains ordered within the FG loop, bound to the Asp212 main chain carbonyl oxygen, and there is no

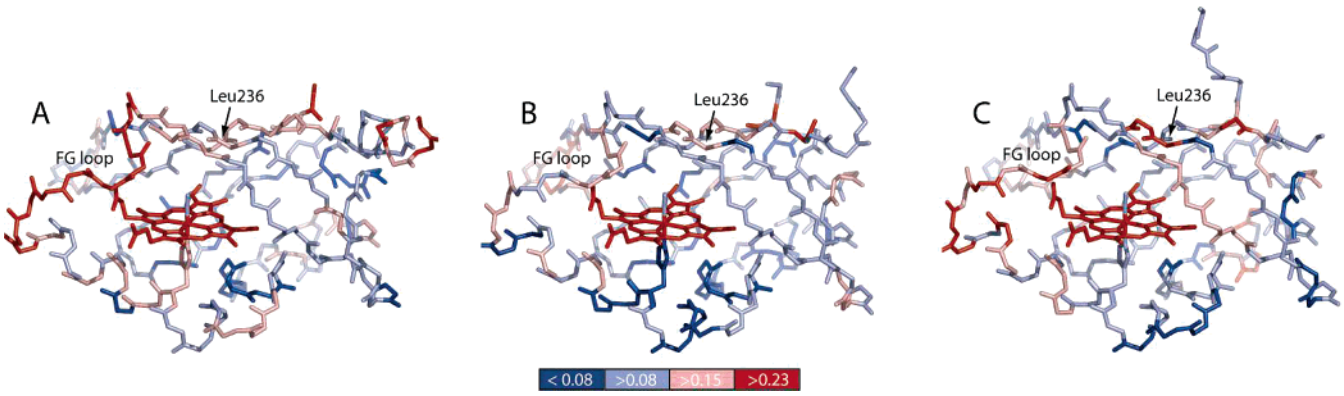

FIGURE 5: Stick models of main chain atoms from the *bj*FixLH *R*32 (A), *C*2A (B), and *C*2B (C) structures. Residues are colored by the magnitude of the average change in atomic position of the three main chain atoms of each residue between the CO and deoxy structures. The scale is in units of angstroms.

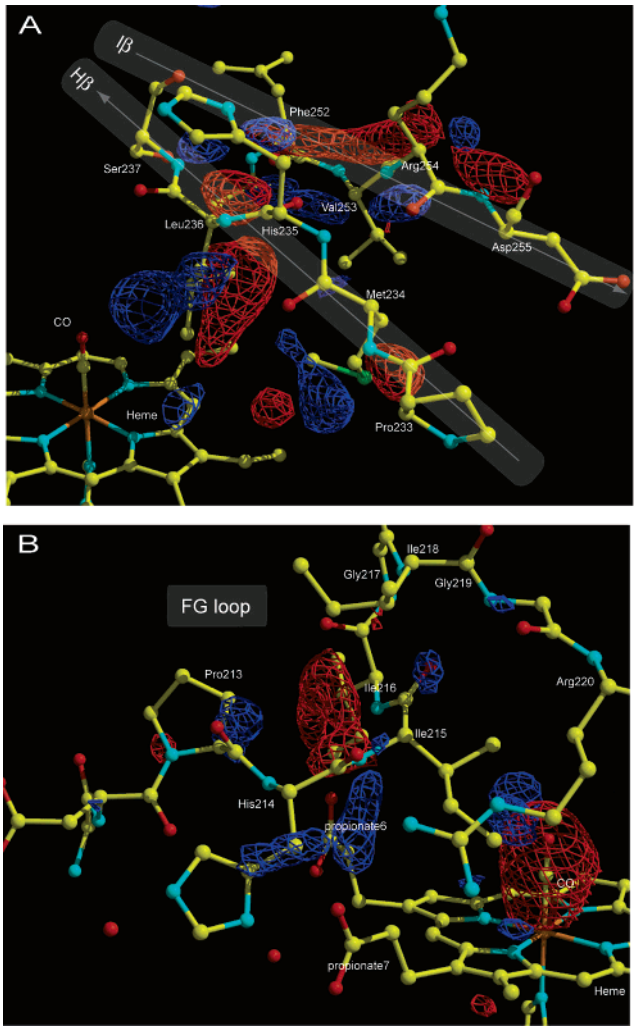

FIGURE 6: F_o(deoxy) − F_o(CO) Fourier difference map of the *R*32 form showing the distal Hβ and Iβ strands (A) and the FG loop region (B) contoured at $\pm 4\sigma$. Negative density is red, and positive density is blue. Structural differences between the liganded and unliganded forms are evident in the FG loop as well as in the Hβ and Iβ strands of the protein.

increase in the temperature factors associated with CO binding. The porphyrin ring, which is shifted both up from the proximal histidine and toward its propionate groups in the *bj*FixLH CO-bound *R*32 and *C*2B models, is instead shifted only upward from the proximal histidine in the *C*2A monomer. Evidently, constraining the loop residues bound to heme propionate 6 gives rise to a rather different motion of the heme in the *C*2A monomer. The second lattice-related difference lies at the interface between the two monomers in the *C*2 form. A CO-induced change in this region, while visible, appears to be modulated by the lattice contacts. Large difference electron density peaks ($\pm 4\sigma$) are visible (Figure 4), though the difference density along the backbone atoms of the I$_\beta$ strand is less continuous than in the *R*32 form. Steric constraints on the side chains of the distal β-sheet residues seem to be the most likely cause of this difference as these side chains are involved in intermolecular contacts between the two monomers in the asymmetric unit. These crystal packing effects may indicate why our monoclinic crystals become noticeably more fragile after reduction and addition of CO. Previous studies of dimeric *sm*FixLH reported similar difficulty in producing ligand-bound crystals (*21*). Thus, the *R*32 crystal form provides the least constrained view of structural differences between the CO and deoxy states of *bj*FixLH.

DISCUSSION

Leu236 Is an Important Ligand-Sensing Side Chain. The FG loop switch has been proposed as the structural signal responsible for catalytic control of the kinase domain in response to ligand binding at the heme domain (*18*−*20*). CO binding does not elicit this switch yet retains some inhibition of FixL activity (*16*, *18*), which implies that the switch is not the sole structural player in ligand recognition. Our results suggest that the Leu236 residue, by sterically occluding the binding pocket, plays a critical role by acting as a general ligand detector. The location of the side chain is sensitive to any ligand bound at the heme, and the region surrounding this residue shows the most substantial differences in electron density upon binding of CO in *bj*FixLH. These differences, though small in magnitude, propagate out from the heme across the distal H$_\beta$ and I$_\beta$ strands more than 15 Å from the heme iron to the C-terminal helix of the *R*32 model, a helix that is not part of the conserved PAS fold. Leu236 is conserved across FixL proteins and has been shown to be essential for proper heme incorporation (*23*, *41*). Thus, this residue fulfills important criteria for participating in signaling. It is conserved; it directly senses the signal (here, ligand binding), and it initiates structural changes that propagate over a long distance to the surface of the domain.

The residues of the H$_\beta$ and I$_\beta$ strands have been implicated in signal transduction in a number of other PAS domain

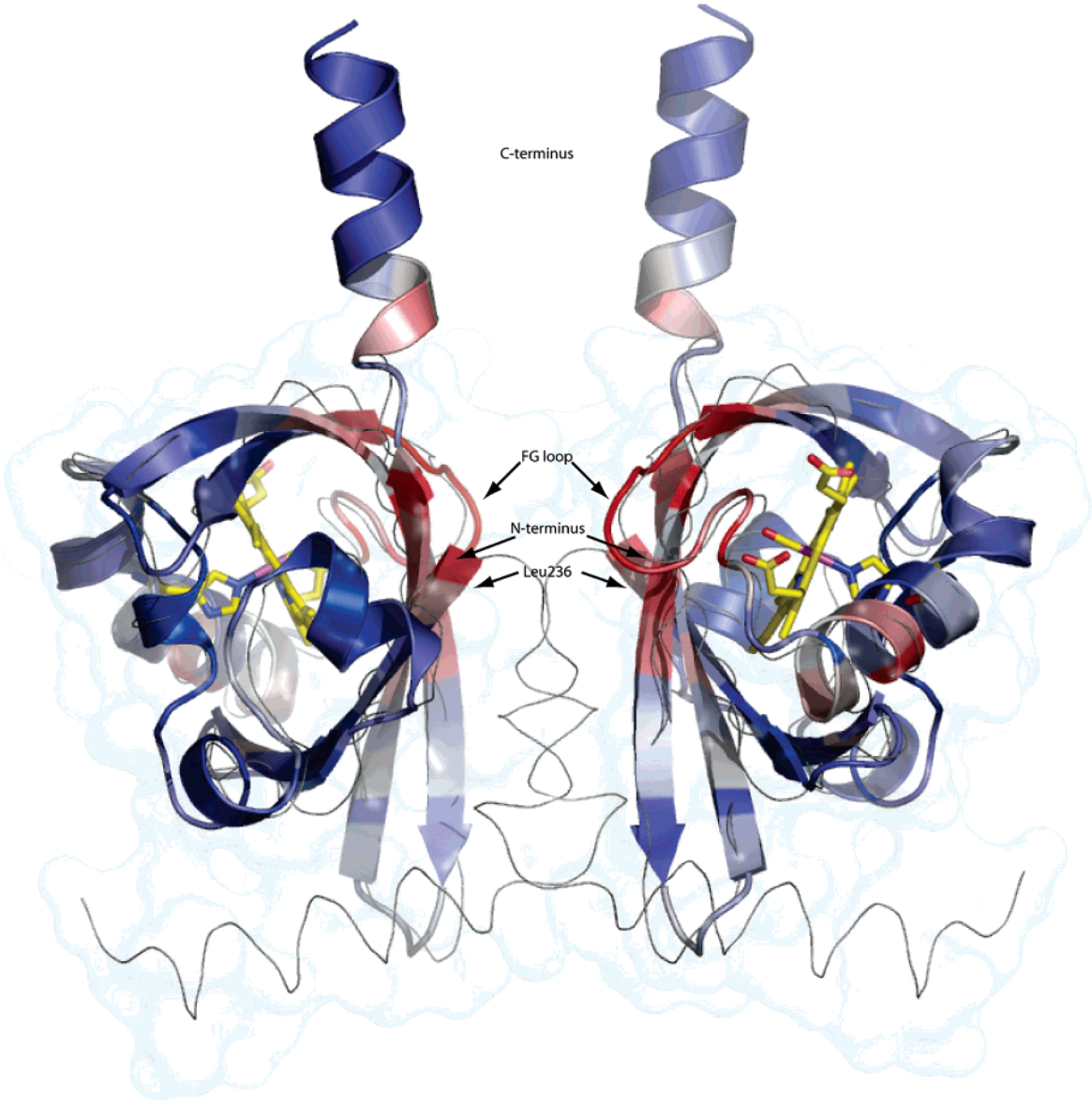

FIGURE 7: Ribbons model of *bj*FixLH from the *R*32 form aligned against the dimeric structures of *sm*FixLH and *ec*DOSH (PDB entries 1D06 and 1V9Y). The ribbon is colored by displacement of main chain atoms between the CO and deoxy states. Residues displaced by binding of CO are at the interface of the dimer near the C-terminus. The thread diagram and surface of the *sm*FixLH dimer are superimposed in gray. The dimer was created by applying the symmetry of the *sm*FixLH crystals to PDB entry 1D06 as described by Miyatake et al. (*21*). The color scale is that from Figure 5.

proteins of diverse function (*42*−*46*). CO-induced regulation of FixL kinase activity may occur by a mechanism similar to that described for the photoreceptor LOV2 (*44*), in which the conformation of a C-terminal helix is altered through its light-dependent interactions with the H_β and I_β strands. As in CO-bound FixLH, the structural changes attributed to signal recognition in LOV2 and PAS kinase do not involve large-scale structural change, yet are sufficient to disrupt interactions at the surface of the molecule along the H_β and I_β strands (*42*, *44*). Recently, a conformational change in the H_β and I_β strands has been implicated in the catalytic control of another bacterial heme-based PAS protein domain, the *Escherichia coli* protein *ec*DOSH (*45*, *46*). These residues are involved in the dimerization interface of *ec*DOSH, whose dimeric structure is similar to that of *sm*FixLH, a closely related FixL whose sequence is 58% identical to that of *bj*FixLH. Kurokawa and colleagues (*45*) describe a scissor-like hinge motion in the heme−PAS domain upon ligation of a critical methionine to the heme in *ec*DOSH, which could alter the relative proximity of the enzymatic domains. Park et al. (*46*) independently identified this motion in *ec*DOS and proposed that it might also occur in *bj*FixLH by means of Arg220 binding to the heme-bound ligand. The distal residues whose positions are most affected by binding of CO are poised at a conserved PAS domain interaction surface in our structures (*43*), which is likely to be the dimerization interface of FixLH (Figure 7), as inferred from the dimeric structures of *sm*FixLH and *ec*DOSH (*21*, *45*) (PDB entries 1D06 and 1V9Y, respectively). This is an especially appealing mechanism for FixL proteins since phosphorylation in the histidine kinase domain occurs in trans (*2*). A hinge motion of the N-terminal PAS domains upon ligand binding may reorient the two C-terminal enzymatic domains in a manner that inhibits phosphorylation.

Effect of Carbon Monoxide Binding on the FG Loop of bjFixLH. Diatomic oxygen, the physiological ligand of

*bj*FixLH, requires the Arg220 residue to bind to the heme iron (*17*). The structural process by which this side chain enters the heme pocket to stabilize the bound oxygen is driven by flattening of the heme and motion of the porphyrin upon ligation, which frees Arg220 to move into the heme pocket (*20*). In our CO-bound structures, heme flattening upon binding CO is transmitted to the FG loop via the hydrogen bond between propionate 6 and Ile216, yet Arg220 fully maintains its salt bridge to propionate 7; the positions of both Arg220 and propionate 7 are unchanged by CO binding. The side chain of Arg206, which has been proposed to compensate for the negatively charged propionate 7 upon loss of Arg220 (*18*−*20*), is disordered by binding of CO in our structures. The movement of propionate 6 and of the FG loop is the likely driving force for releasing this residue. In this view, the CO-bound state represents an intermediate in the FG switch mechanism, poised at the point where Arg220 is able to select against the heme-bound ligand. Previous studies noted no change in the position of this Arg206 side chain for the CO-bound state, but did observe a change for the NO-bound state for *bj*FixLH (*19*). Evidently, neither heme flattening nor the availability of the compensating Arg206 side chain is sufficient to free the side chain of Arg220; thus the electrostatics of the ligand must play the role of releasing the arginine from the propionate. We detect a change in the position of Ile215, Ile216, and Gly217 in the FG loop caused by doming of the heme. While this change is not of the magnitude of the FG loop switch seen in the oxy and CN-met structures, we do not rule out its significance in CO-induced inhibition of FixL. Mutagenesis studies have implicated residues Ile215 and Ile216 in ligand recognition, both of which are highly conserved in FixLs (*23*). From our structures, it is not evident why these residues are so important. Ile215 easily accommodates bound CO with little steric clash; its hydrogen bond to propionate 6 that drives FG loop motion involves its backbone amide, though the side chain of Ile215 interacts with the aliphatic region of the side chain of Arg220 in the oxy state. The Ile216 side chain faces into solvent. Thus, it is not possible to address the role of these residues in the context of the isolated CO−*bj*FixLH heme−PAS domain. Ligand-sensitive dynamics of the FG loop have been suggested as a catalytic control mechanism for the heme−PAS domains (*17*). Indeed, the shift of propionate 6 and Ile216 upon CO binding gives rise to altered temperature factors in this region, and changes in dynamics of the FG loop of the protein have also been described for methionine ligation in *ec*DOSH (*46*).

Ensemble Ligand Detection. Prior studies implicated the FG loop switch as the region of the protein that is sensitive to ligand binding and transmits a signal (*18*−*21*, *23*). Our results suggest that the structural signaling mechanism in *bj*FixLH is more complex, is not restricted to a single region of the protein, and may display redundant or semiredundant aspects. As in CO-bound *bj*FixLH, inhibition of CN-bound R220A *bj*FixLH mutants has been observed in the apparent absence of the FG loop switch (*17*). Examination of the oxy and CN−*bj*FixLH structures (*18*) (PDB entries 1DP6 and 1LT0, respectively) reveals that the Arg220-dependent FG loop switch and structural change in the β-sheet distal to the heme produced by Leu236 are most likely coupled across the β-sheet of the protein. Movement of Arg220 into the heme pocket in the CN- and O_2-bound structures causes a substantial change in the position of the Arg220 backbone atoms, and these are hydrogen bonded from G_β to the main chain atoms of residue Leu236 in the I_β strand, the residue we note as a candidate ligand sensor. Thus, the movement of several residues is redundantly linked to respond to ligand binding. This coupling allows the FG loop, Arg220, and the distal β-residues to act as a group; Leu236 is displaced by the bound ligand, which shifts the residues of the H_β and I_β strands while propionate 6 shifts Ile215 to Ile218 of the FG loop. This provides greater conformational freedom to the main chain atoms of Arg220, and enables its side chain to move into the ligand pocket, which results in further displacement of the distal β-sheet residues. These structural changes in the protein depend directly on three characteristics of the bound ligand: ligand field strength via doming of the heme and subsequent propionate 6 movement, ligand charge or polarizability sensed by movement of Arg220 into the heme pocket, and ligand shape sensed by steric clash of Leu236 with the bound ligand. Ligands that best meet the three criteria, namely, O_2 and CN, create the largest conformational change throughout the β-sheet surface of *bj*FixLH. This gives rise to substantial inhibition of the kinase activity by an as yet unknown mechanism that may involve a quaternary structural change in the protein dimer such as that described by Kurokawa et al. (*45*). CO and NO only partially meet these criteria and create modest conformational differences that weakly inhibit the kinase.

CONCLUSIONS

We have examined the structures of CO-bound *bj*FixLH in *R*32 and *C*2 crystal forms using F_o(deoxy) − F_o(CO) difference maps to elucidate the small structural changes associated with binding of CO to investigate the mechanism of kinase inhibition by weak ligands. These maps show a shift of the residues of the H_β and I_β strands upon CO binding, driven by the steric interaction between the ligand and the side chain of Leu236. This structural change occurs in the distal residues of the β-sheet in a region noted to be involved in regulation in PAS domains. In the FG loop of the protein, there is a shift driven by propionate 6 of the heme group with a change in the spin state, and though the FG loop switch does not occur, Arg206 becomes disordered and loop temperature factors are increased. Finally, we note the interaction between Leu236 and Arg220, the distal coordinating residue of oxygen in *bj*FixLH, and propose that the action of these residues is coupled to the sense-bound ligand by creating structural change on the distal side of the β-sheet. This occurs in a region that is consistent with other PAS domains, suggesting that signal generation within these domains is conserved. Ligand binding is likely to alter the quaternary structure of the FixLH dimer, as has been reported for the related protein *ec*DOSH. Structures of the intact, full-length dimeric proteins are necessary for a complete understanding of signaling in these molecules.

ACKNOWLEDGMENT

We would like to acknowledge Marie-Alda Gilles-Gonzalez for the *bj*FixLH plasmid and helpful scientific discussion. J.K. thanks Sean Crosson and Sudarshan Rajagopal for their assistance with this work. Supported by NIH Grants GM036452 and RR07707 (BioCARS) to K.M.

REFERENCES

1. Sciotti, M. A., et al. (2003) Disparate oxygen responsiveness of two regulatory cascades that control expression of symbiotic genes in *Bradyrhizobium japonicum*, *J. Bacteriol. 185* (18), 5639−5642.
2. West, A. H., and Stock, A. M. (2001) Histidine kinases and response regulator proteins in two-component signaling systems, *Trends Biochem. Sci. 26* (6), 369−376.
3. de Philip, P., et al. (1992) Modular structure of the FixL protein of *Rhizobium meliloti*, *Mol. Gen. Genet. 235* (1), 49−54.
4. Pellequer, J. L., Brudler, R., and Getzoff, E. D. (1999) Biological sensors: More than one way to sense oxygen, *Curr. Biol. 9* (11), R416−R418.
5. Zhulin, I. B., Lois, A. F., and Taylor, B. L. (1995) Behavior of *Rhizobium meliloti* in oxygen gradients, *FEBS Lett. 367* (2), 180−182.
6. Nambu, J. R., et al. (1991) The *Drosophila* single-minded gene encodes a helix-loop-helix protein that acts as a master regulator of CNS midline development, *Cell 67* (6), 1157−1167.
7. Huang, Z. J., Edery, I., and Rosbash, M. (1993) PAS is a dimerization domain common to *Drosophila* period and several transcription factors, *Nature 364* (6434), 259−262.
8. Hoff, W. D., et al. (1994) Thiol ester-linked *p*-coumaric acid as a new photoactive prosthetic group in a protein with rhodopsin-like photochemistry, *Biochemistry 33* (47), 13959−13962.
9. Gilles-Gonzalez, M. A., Ditta, G. S., and Helinski, D. R. (1991) A haemoprotein with kinase activity encoded by the oxygen sensor of *Rhizobium meliloti*, *Nature 350* (6314), 170−172.
10. Christie, J. M., et al. (1999) LOV (light, oxygen, or voltage) domains of the blue-light photoreceptor phototropin (nph1), binding sites for the chromophore flavin mononucleotide, *Proc. Natl. Acad. Sci. U.S.A. 96* (15), 8779−8783.
11. Delgado-Nixon, V. M., Gonzalez, G., and Gilles-Gonzalez, M. A. (2000) Dos, a heme-binding PAS protein from *Escherichia coli*, is a direct oxygen sensor, *Biochemistry 39* (10), 2685−2691.
12. Chang, A. L., et al. (2001) Phosphodiesterase A1, a regulator of cellulose synthesis in *Acetobacter xylinum*, is a heme-based sensor, *Biochemistry 40* (12), 3420−3426.
13. Dioum, E. M., et al. (2002) NPAS2: A gas-responsive transcription factor, *Science 298* (5602), 2385−2387.
14. Gilles-Gonzalez, M. A., and Gonzalez, G. (1993) Regulation of the kinase activity of heme protein FixL from the two-component system FixL/FixJ of *Rhizobium meliloti*, *J. Biol. Chem. 268* (22), 16293−16297.
15. Gilles-Gonzalez, M. A., Gonzalez, G., and Perutz, M. F. (1995) Kinase activity of oxygen sensor FixL depends on the spin state of its heme iron, *Biochemistry 34* (1), 232−236.
16. Tuckerman, J. R., et al. (2002) Ligand and oxidation-state specific regulation of the heme-based oxygen sensor FixL from *Sinorhizobium meliloti*, *Biochemistry 41* (19), 6170−6177.
17. Dunham, C. M., et al. (2003) A distal arginine in oxygen-sensing heme-PAS domains is essential to ligand binding, signal transduction, and structure, *Biochemistry 42* (25), 7701−7708.
18. Gong, W., Hao, B., and Chan, M. K. (2000) New mechanistic insights from structural studies of the oxygen-sensing domain of *Bradyrhizobium japonicum* FixL, *Biochemistry 39* (14), 3955−3962.
19. Gong, W., et al. (1998) Structure of a biological oxygen sensor: A new mechanism for heme-driven signal transduction, *Proc. Natl. Acad. Sci. U.S.A. 95* (26), 15177−15182.
20. Hao, B., et al. (2002) Structure-based mechanism of O_2 sensing and ligand discrimination by the FixL heme domain of *Bradyrhizobium japonicum*, *Biochemistry 41* (43), 12952−12958.
21. Miyatake, H., et al. (2000) Sensory mechanism of oxygen sensor FixL from *Rhizobium meliloti*: Crystallographic, mutagenesis and resonance Raman spectroscopic studies, *J. Mol. Biol. 301* (2), 415−431.
22. Perutz, M. F., Paoli, M., and Lesk, A. M. (1999) FixL, a haemoglobin that acts as an oxygen sensor: Signaling mechanism and structural basis of its homology with PAS domains, *Chem. Biol. 6* (11), R291−R297.
23. Mukai, M., et al. (2000) Roles of Ile209 and Ile210 on the heme pocket structure and regulation of histidine kinase activity of oxygen sensor FixL from *Rhizobium meliloti*, *Biochemistry 39* (45), 13810−13816.
24. Gilles-Gonzalez, M. A., et al. (1994) Heme-based sensors, exemplified by the kinase FixL, are a new class of heme protein with distinctive ligand binding and autoxidation, *Biochemistry 33* (26), 8067−8073.
25. Chen, Y., et al. (1994) Optical Monitoring of Protein Crystals in Time-Resolved X-ray Experiments: Microspectrophotometer Design and Performance, *Rev. Sci. Instrum. 65* (5), 1506−1511.
26. Otwinowski, Z., and Minor, W. (1997) Processing of X-ray diffraction data collected in oscillation mode, *Macromol. Crystallogr. 276* (Part A), 307−326.
27. Kissinger, C. R., Gehlhaar, D. K., and Fogel, D. B. (1999) Rapid automated molecular replacement by evolutionary search, *Acta Crystallogr. D55*, 484−491.
28. Brunger, A. T., et al. (1998) Crystallography & NMR system: A new software suite for macromolecular structure determination, *Acta Crystallogr. D54* (Part 5), 905−921.
29. Jones, T. A., Zou, J. Y., and Kjeldgaard, M. (1991) A Modeling Environment for Map Interpretation, *Abstracts of Papers of the American Chemical Society*, Vol. 202, 29-Cinf, American Chemical Society, Washington, DC.
30. McRee, D. E. (1992) *J. Mol. Graphics 10*, 44−47.
31. Bailey, S. (1994) The CCP4 Suite: Programs for Protein Crystallography, *Acta Crystallogr. D50*, 760−763.
32. Carson, M. (1997) Ribbons: Macromolecular Crystallography, *Methods Enzymol. 277* (Part B), 493−505.
33. DeLano, W. L. (2002) *The PyMOL Molecular Graphics System*, DeLano Scientific, San Carlos, CA.
34. Peng, S. M., and Ibers, J. A. (1976) Stereochemistry of carbonylmetalloporphyrins. The structure of (pyridine)(carbonyl)(5,10,-15,20-tetraphenylprophinato)iron(II), *J. Am. Chem. Soc. 98* (25), 8032−8036.
35. Scheidt, W. R., et al. (1981) A (carbonmonoxy)heme complex with a weak proximal bond. Molecular stereochemistry of carbonyl(deuterioporphinato)(tetrahydrofuran)iron(II), *Biochemistry 20* (12), 3653−3657.
36. Lim, M., Jackson, T. A., and Anfinrud, P. A. (1995) Binding of CO to myoglobin from a heme pocket docking site to form nearly linear Fe−C−O, *Science 269* (5226), 962−966.
37. Kachalova, G. S., Popov, A. N., and Bartunik, H. D. (1999) A steric mechanism for inhibition of CO binding to heme proteins, *Science 284* (5413), 473−476.
38. Vojtechovsky, J., et al. (1999) Crystal structures of myoglobin-ligand complexes at near-atomic resolution, *Biophys. J. 77* (4), 2153−2174.
39. Miyatake, H., et al. (1999) Iron coordination structures of oxygen sensor FixL characterized by Fe K-edge extended X-ray absorption fine structure and resonance Raman spectroscopy, *J. Biol. Chem. 274* (33), 23176−23184.
40. Henderso, R., and Moffat, J. K. (1971) Difference Fourier Technique in Protein Crystallography: Errors and Their Treatment, *Acta Crystallogr. B27*, 1414.
41. Nakamura, H., et al. (1998) Identification of the hydrophobic amino acid residues required for heme assembly in the rhizobial oxygen sensor protein FixL, *Biochem. Biophys. Res. Commun. 247* (2), 427−431.
42. Amezcua, C. A., et al. (2002) Structure and interactions of PAS kinase N-terminal PAS domain: Model for intramolecular kinase regulation, *Structure 10* (10), 1349−1361.
43. Erbel, P. J., et al. (2003) Structural basis for PAS domain heterodimerization in the basic helix−loop−helix−PAS transcription factor hypoxia-inducible factor, *Proc. Natl. Acad. Sci. U.S.A. 100* (26), 15504−15509.
44. Harper, S. M., Neil, L. C., and Gardner, K. H. (2003) Structural basis of a phototropin light switch, *Science 301* (5639), 1541−1544.
45. Kurokawa, H., et al. (2004) A redox-controlled molecular switch revealed by the crystal structure of a bacterial heme PAS sensor, *J. Biol. Chem.* (in press).
46. Park, H., et al. (2004) Insights into signal transduction involving PAS domain oxygen-sensing heme proteins from the X-ray crystal structure of *Escherichia coli* Dos heme domain (Ec DosH), *Biochemistry 43* (10), 2738−2746.

BI047942R